

# Cylindrical nanochannels in ion-track polycarbonate membranes studied by small-angle X-ray scattering

G rard P py,<sup>a,b\*</sup> Peter Boesecke,<sup>c</sup> Alexandr Kuklin,<sup>d</sup> Emmanuel Manceau,<sup>a</sup> Birgitta Schiedt,<sup>e</sup> Zuzanna Siwy,<sup>e,f</sup> Marcel Toulemonde<sup>g</sup> and Christina Trautmann<sup>e</sup>

<sup>a</sup>Laboratoire L on Brillouin (LLB), CEA Saclay, 91191 Gif sur Yvette, Cedex, France, <sup>b</sup>Institute for Solid State Physics, SzFKI, POB 49, H-1525 Budapest, Hungary, <sup>c</sup>European Synchrotron Radiation Facility (ESRF), 38043 Grenoble, Cedex, France, <sup>d</sup>FLNP, JINR, 141980 Dubna, Russia, <sup>e</sup>Gesellschaft f r Schwerionenforschung (GSI), Planckstr. 1, 64291 Darmstadt, Germany, <sup>f</sup>University of California, Irvine, CA 92697, USA, and <sup>g</sup>CIRIL, BP 5133, 14070 Caen, Cedex 5, France. Correspondence e-mail: pepy@dsm-mail.saclay.cea.fr

Different types of polycarbonate foils were irradiated with 1.4 GeV Xe ions, ultra-violet (UV) treated and subsequently etched, creating cylindrical pores of high aspect ratio. The pores are perfectly well aligned and represent excellent objects for small-angle X-ray scattering. Two-dimensional scattering spectra exhibit highly anisotropic patterns with clear presentation of numerous oscillations of the Bessel function, the radial part of the scattering function. Modelling the pores as parallel cylinders allows us to deduce the pore radius and the radius dispersion as a function of UV treatment, etching time and fluence. It is demonstrated that the UV treatment has a beneficial influence on the pore-size distribution, in particular for small pores.

  2007 International Union of Crystallography  
Printed in Singapore – all rights reserved

## 1. Introduction

By irradiating polymer foils with energetic heavy ions and subsequent etching of the ion tracks, porous membranes are produced (so called ion-track membranes). Although used in numerous scientific and technological fields (Spohr, 1980; Metz *et al.*, 2004; Reber *et al.*, 1999; Yoshida *et al.*, 1997), filtration is probably one of the most popular applications. Over the many years, pore fabrication was extended to different polymer materials and the size of the pores became smaller and smaller. To date, pores with diameters from tens to hundreds of nanometres are used as templates for the fabrication of single- and multi-crystalline nanowires of materials such as metals, semiconductors and insulators (Ferain & Legras, 2003; Chtanko *et al.*, 2005; Dobrev *et al.*, 2005). These wires are attracting much attention due to their potential applications in electronic, sensoric, optoelectronic and thermoelectric devices (Cornelius *et al.*, 2005). Various groups have started to use single conical pores with very small diameters (Siwy *et al.*, 2003, 2002) as sensors for single molecules, *e.g.* desoxyribonucleic acid (DNA) (Heins *et al.*, 2005; Mara *et al.*, 2004; Schiedt *et al.*, 2005).

For all these applications it is crucial to understand the pore forming process well and to create highly uniform pores with high reproducibility. For this, the etching behaviour of individual ion tracks should be as similar as possible. A most suitable method for testing the properties of a large pore ensemble is provided by small-angle X-ray scattering (SAXS) (P py & Kuklin, 2001; P py *et al.*, 2003); it is non-destructive and analyses a large number of pores with a single measurement. Moreover, SAXS provides three-dimensional pore information in the bulk, in contrast to typical microscopy techniques (*e.g.* scanning electron or force microscopy) that are limited to the sample surface.

In this study, pores in ion-track membranes of two types of polycarbonate are compared. We investigated the pore size and the size

distribution as a function of etching time, UV treatment and pore density.

## 2. Experimental

### 2.1. Ion irradiation and track etching

As membranes we used two different types of amorphous polycarbonate foils (provided by Bayer, Germany), 30  $\mu\text{m}$  thick Makrofol N and 20  $\mu\text{m}$  thick LOFO. The foils were irradiated at the linear accelerator UNILAC at Gesellschaft f r Schwerionenforschung (GSI Darmstadt, Germany) with Xe ions of 1.4 GeV energy. The range of the ions is more than 150  $\mu\text{m}$  and thus much larger than the foil thickness. Samples of a few  $\text{cm}^2$  in size were exposed normal to the surface to fluences of  $3 \times 10^8$ ,  $5 \times 10^8$  and  $1 \times 10^9$  ions  $\text{cm}^{-2}$ . Subsequent to the ion irradiation, half of the samples were exposed to UV light for 1 h on each side. This is a typical treatment in order to enhance preferential etching of ion tracks (Ferain & Legras, 2003). By immersing the samples in a suitable chemical agent, the damaged zone along the ion track is dissolved at a faster rate than the surrounding polymer matrix, creating quasi-cylindrical pores. Their diameter is adjusted by the etching time (Fleischer *et al.*, 1975; Spohr, 1980). As etchant we used 5 M aqueous NaOH at 333 K. The duration was 3, 5 and 8 min, producing pore diameters between ~30 and 170 nm (Fig. 1).

### 2.2. Small-angle X-ray scattering experiments

The track-etched membranes were analysed by small-angle X-ray scattering at the ID01 beamline at the European Synchrotron Research Facility (ESRF, Grenoble, France). The sample foils were fixed on a holder and covered with a 10  $\mu\text{m}$  thick mica sheet (Jahre GmbH, Berlin) to improve their flatness. Using a goniometer head allowed us to rotate the sample holder around the vertical and the

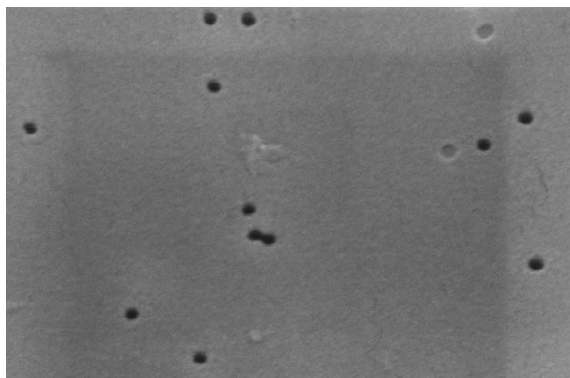


**Figure 1**  
Surface electronic micrograph (SEM) of a LOFO sample irradiated with  $3 \times 10^8$  Xe ions  $\text{cm}^{-2}$ , UV treated and etched for 5 min in 5 M NaOH at 333 K (courtesy of S. Poissonnet and P. Bonnaillie, DMN/SRMP, CEA-Saclay).

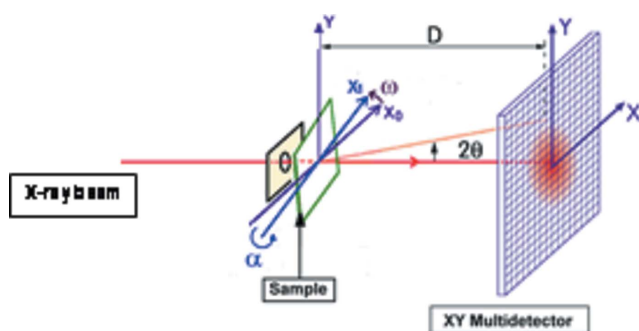


**Figure 2**  
Scheme of the SAXS experiment including the sample mounted on a goniometer head and the two-dimensional detector for the scattered X-rays. The nanochannels are perpendicular to the polymer foil. Using the  $\omega$  tilt angle of the goniometer, the sample foil is oriented in such a way that the channel axis is inside the horizontal plane, at an angle  $\alpha$  to the main beam.

horizontal axes (Fig. 2). The incoming X-ray beam was monochromated to a wavelength of  $\lambda = 0.088$  nm. The scattered X-rays penetrated through a beryllium window into a vacuum chamber containing a position-sensitive detector. The sample-to-detector distance is variable and was adjusted to three different positions: 0.7, 2.0 and 4.0 m. As a detector we used a Princeton charge coupled device (CCD) camera with  $1242 \times 1152$  pixels of  $63.3 \times 63.3$   $\mu\text{m}$  each.

As the length of the pores is much bigger than their radius, the scattering is extremely sensitive to the orientation of the channel axis with respect to the X-rays. It is preferable that the channel axis lies in the horizontal scattering plane (Pépy & Kuklin, 2001). In a typical experiment, this was obtained by tilting the sample on the goniometer head with respect to the X-ray beam and scanning around the horizontal axis until the scattering pattern became symmetric in the horizontal plane. Once the nanochannels were aligned, the sample was rotated in small steps around the vertical axis, recording a scattering image for each step. Before the rotational scan, a dark current image was measured as a background file. For final analysis of the X-ray scattering patterns, the data files were corrected by the CCD dark current and field flatness and were calibrated by the X-ray intensity as given by the ESRF protocol.

### 3. Analysis

Given the stochastic distribution of the pores, their distance correlation is negligible and the scattering intensity can be interpreted as the incoherent sum of the scattering contributions of individual pores. The scattering experiment provides therefore the mean value averaged over the pore ensemble of each sample. When analyzing the scattering data, we have to compare the measured intensity distribution on the detector with calculations performed assuming a certain size and geometry of the scattering object. Object parameters which give best agreement with the experimental scattering data are deduced as most reliable. Note that the agreement has to be achieved with the same parameter set for all rotation angles between the pore axis and the primary X-ray beam.

The nanopores in the membrane are modelled by extended straight cylinders with radius  $R$  and half-length  $L$ . The form factor for scat-

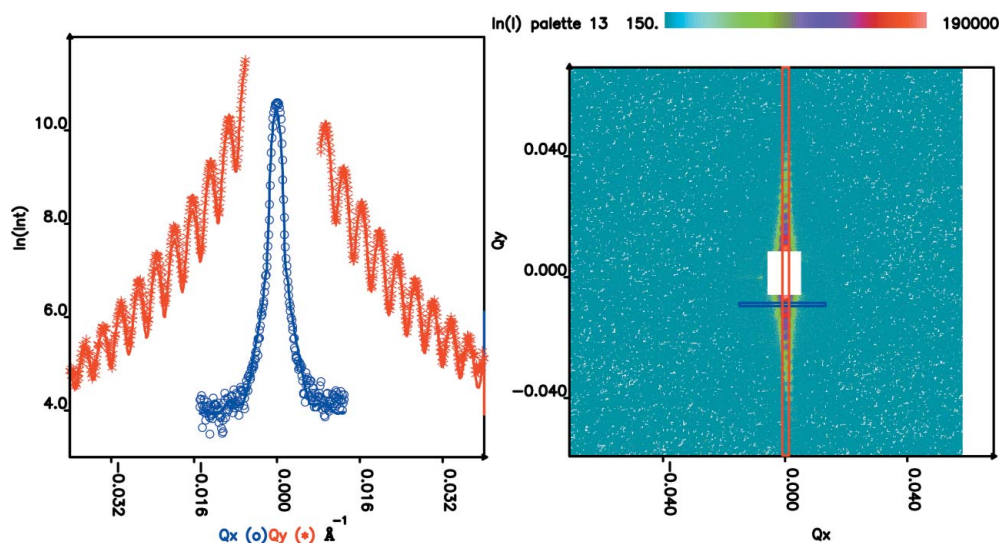


**Figure 3**  
Right: Scattering pattern of LOFO foil irradiated with  $3 \times 10^8$  ions  $\text{cm}^{-2}$ , UV sensitized and etched for 8 min. The sample was tilted vertically by  $-4.5^\circ$  with respect to the X-ray beam. The data pixels in the central square are removed because they correspond to the beam stopper for the primary X-ray beam. Left: The scattering intensity is analyzed as a function of the scattering vector by plotting the pixel intensity along the narrow vertical (stars) and horizontal (circles) rectangular shaped filters. In the model calculation (solid lines), the pores are described by straight cylinders with the radius and the length of the pore as free-fit parameters (including an adjustable size distribution). Each pixel intensity is modelled individually according to equations (4) and (5) (Pépy, 2007). The left picture is a projection on the relevant axis of the data and calculated points, after a two-dimensional fit.

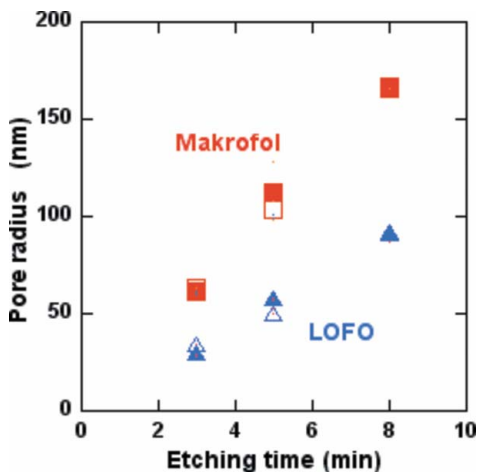


**Figure 4** Pore radius as a function of etching time for Makrofol N and LOFO polycarbonate membranes irradiated with  $3 \times 10^8$  Xe ions  $\text{cm}^{-2}$  and etched in 5 M NaOH at 333 K; with (full symbols) and without (open symbols) UV treatment.

tering by a single cylinder, described with the cylinder coordinates  $r$  and  $\varphi$ , and with  $z$  as cylinder axis, is given by

$$A(\mathbf{Q}, R, L) = \int_{-L}^L \int_0^R \int_0^{2\pi} C \exp[-i(Q_r r \cos \varphi + Q_z z)] d\varphi dr dz, \quad (1)$$

where  $\mathbf{Q}$  denotes the scattering vector,  $Q_r$  and  $Q_z$  are the respective radial and longitudinal components, and  $C$  is a scalar coefficient proportional to the scattering contrast and the fluence; the modulus of the scattering vector is  $Q = (4\pi/\lambda) \sin(\theta/2)$  where  $\lambda$  is the X-ray wavelength and  $\theta$  is the scattering angle. After performing the integration, the form factor becomes

$$A(\mathbf{Q}, R, L) = 2\pi CLR^2 \frac{\sin(Q_z L)}{Q_z L} \frac{J_1(Q_r R)}{Q_r R}, \quad (2)$$

where  $J_1$  describes the radial part of the scattering function by a Bessel function of first-order.

The scattering intensity is

$$I(\mathbf{Q}, R, L) = |A(\mathbf{Q}, R, L)|^2. \quad (3)$$

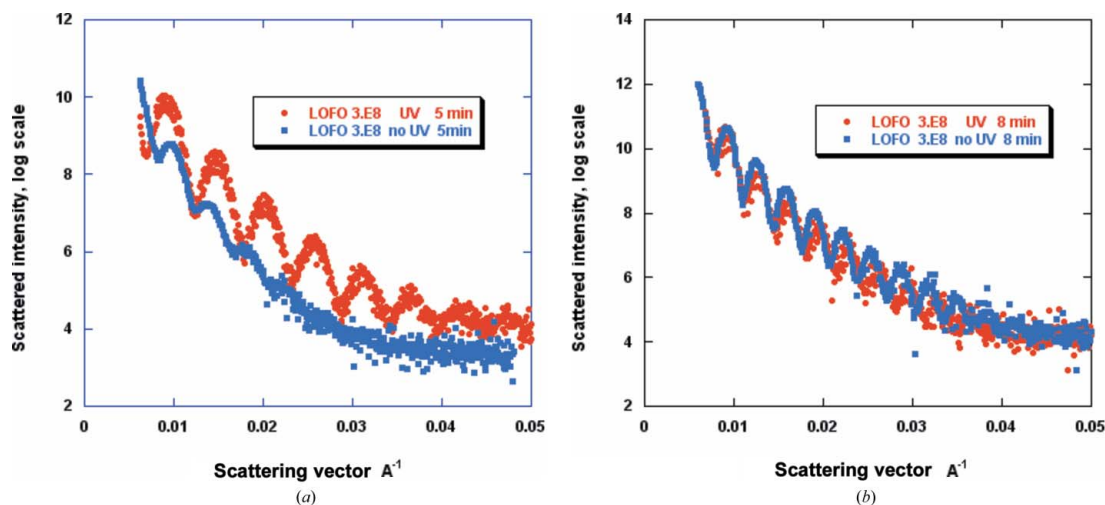


**Figure 5** SAXS intensity as a function of scattering vector for LOFO samples (irradiated with  $3 \times 10^8$  Xe ions  $\text{cm}^{-2}$ ) etched for 5 min (left) and for 8 min (right). In particular for small pores (left), UV-sensitized samples (red) exhibit much better resolved oscillations than untreated samples (blue).

In real samples, the situation is more complicated, because the pores have a dispersion in radius and in length. In the model, we assumed the length dispersion  $p_{LG}$  to be Gaussian, whereas for the radius dispersion  $p_{Rln}$ , a log normal probability law seems to be better than a Gaussian. With these modifications the scattering intensity reads as

$$I(\mathbf{Q}, R_0, L_0) = \int_0^\infty p_{Rln}(R_0, R) dR \int_{-\infty}^\infty p_{LG}(L_0, L) dL |A(\mathbf{Q}, R, L)|^2, \quad (4)$$

with

$$p_{LG}(L_0, L) = \frac{1}{\sigma_{LG}(2\pi)^{1/2}} \exp\left[-\frac{(L - L_0)^2}{2\sigma_{LG}^2}\right]$$

and

$$p_{Rln}(R_0, R) = \frac{1}{(R/R_0)\sigma_{Rln}(2\pi)^{1/2}} \exp\left\{-\frac{[\ln(R/R_0)]^2}{2\sigma_{Rln}^2}\right\}, \quad (5)$$

where  $\sigma_{LG}$  and  $\sigma_{Rln}$  characterize the distribution width around the pore length  $L_0$  and around the radius  $R_0$ , respectively.

A complete calculation of the scattering intensity for all pixels and for the many images of the different rocking curves would be time consuming. We therefore analysed mainly scattering patterns where the axis of the pores were tilted by a few degrees with respect to the incoming X-ray beam. Under this condition, the scattering pattern on the two-dimensional detector is highly anisotropic, exhibiting two symmetric streaks whose intensity is large close to the detector centre and decreases at greater scattering angles (Fig. 3, right). The data are analysed by selecting a narrow rectangular-shaped filter as indicated in the scattering pattern of Fig. 3 (right). The pixel intensity of the selected filter area is plotted as a function of the vertical and/or horizontal axis.

The intensity along the vertical detector axis is characterized by oscillations resulting from the Bessel functions [equation (2)]. The very high resolution of the oscillations is a clear indication that the pores are very uniform, *i.e.*, their radial dispersion is small and they are well aligned with respect to each other. This latter property is not too surprising because of the small divergence of the ion beam producing the tracks. The distance between two oscillations scales with the inverse of the pore radius. The finite apparatus resolution leads to a damping of fixed value, whereas damping related to a

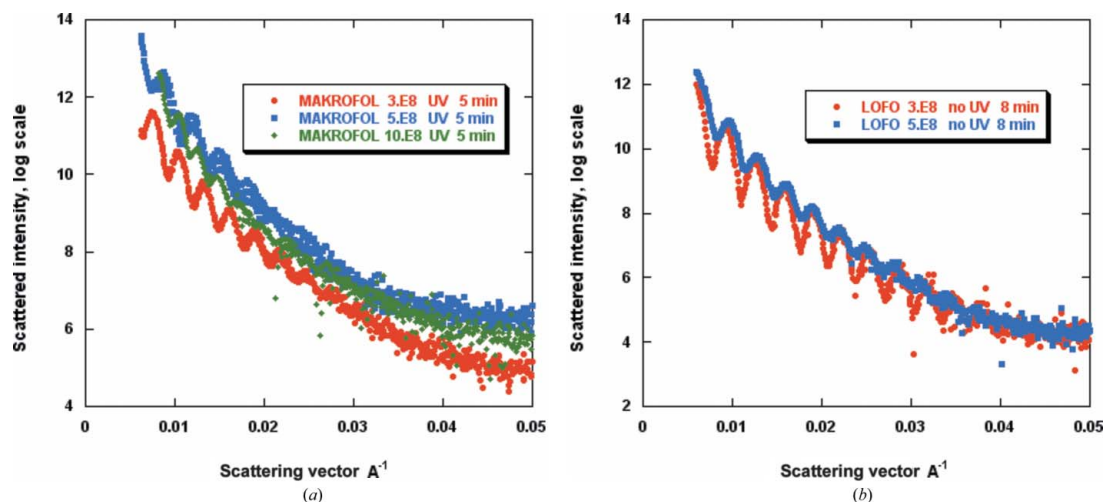


**Figure 6**  
SAXS intensity as a function of scattering vector (left) for Makrofol samples (UV treated, etched for 5 min) and (right) for LOFO samples (without UV, etched for 8 min) irradiated with different fluences. With increasing pore densities, the oscillations smear out.

dispersion of the pore radii increases with the scattering angle. The width of the intensity data from the horizontal direction (central data in Fig. 3, left) scales with the inverse of the pore length.

To analyse quantitatively the scattering pattern of the different membranes, the scattering intensity of cylindrical objects with variable pore parameters is calculated. In order to describe the damping of the strong oscillations, it was necessary to introduce also the pore length as a free parameter having a certain dispersion and being equal to or smaller than the foil thickness. The best fit to the experimental SAXS data fixes the free parameters and finally gives us the mean radius of the pore and its radial dispersion.

## 4. Results

### 4.1. Pore radius and etching time

Applying the model described above, the pore sizes of membranes of different fluences and etching times was deduced. Fig. 4 displays the data for foils irradiated with  $3 \times 10^8$  ions  $\text{cm}^{-2}$ , with and without UV treatment. The radial etching rate is about 21 and 12  $\text{nm min}^{-1}$  for Makrofol and LOFO, respectively. The UV treatment does not show any significant influence on the pore size.

### 4.2. UV sensitization and pore size distribution

To test the influence of UV treatment prior to chemical track etching, we compared spectra of identical samples with and without UV sensitization. As illustrated in Fig. 5, there is a strong effect on the clearness, total number and damping of the oscillations. The effect is stronger for smaller pores and more effective for LOFO than for Makrofol. Most fits to the data of UV-sensitized samples do not require the inclusion of a radial pore-size distribution, whereas without UV sensitization, the radius dispersion is typically a few per cent. Best fit values, for example, for a LOFO sample etched for 5 min (Fig. 5, right) yield a pore radius of  $R = 57.7$  nm, no radius dispersion (with UV) and  $R = 49.4$  nm, dispersion  $\Delta R/R = 5.3\%$  (without UV).

### 4.3. Influence of fluence

The overall porosity of a membrane is a function of the pore density (given by the ion fluence) and the pore size (determined by

the etching process). At large porosities, a significant number of channels may overlap and thus deteriorate; one of the advantages of ion-track membranes compared to other filter materials. The membrane quality can be estimated by calculating the contribution of single and multiple pore overlap using Poisson's law (Riedel & Spohr, 1979). For a fluence of  $3 \times 10^8$   $\text{cm}^{-2}$ , 10% of pores of radius  $R = 155$  nm are calculated to overlap, whereas at a higher fluence of  $10^9$   $\text{cm}^{-2}$ , this occurs already for smaller pores of  $R = 85$  nm. Experimentally, some information about interacting pores can be obtained by analyzing the radial pore dispersion of SAXS data. Note that the reason for radius dispersion is not unambiguous and by no means quantitative. Nevertheless, this analysis is interesting because scattering at two objects is only independent if their distance is a few times larger than their size. Therefore SAXS will reveal interacting objects well before they actually touch each other. Interaction effects by SAXS are indicated clearly before we can detect overlapping pores and this information is not restricted to the membrane surface but concerns the channels through the entire bulk of the films.

Fig. 6 illustrates the fluence effect for a set of LOFO and Makrofol samples irradiated with  $3 \times 10^8$ ,  $5 \times 10^8$  and in the case of Makrofol additionally  $10^9$  ions  $\text{cm}^{-2}$ . Apart from the irradiation, the treatment of the samples of the same material was identical, *i.e.* UV exposure and etching for 5 min for Makrofol, and 8 min etching without UV treatment for LOFO. For the lowest pore density, the oscillations are well defined and can be fitted without any pore size distribution. With increasing pore densities, the oscillations smear out, and we have to include a log normal dispersion (for Makrofol:  $\Delta R/R = 1.2$  for  $5 \times 10^8$  pores  $\text{cm}^{-2}$  and  $\Delta R/R = 2.5\%$  for  $10^9$  pores  $\text{cm}^{-2}$ ) while the radius remains constant.

## 5. Conclusion

The properties of ion-track membranes with etched pores in two different amorphous polycarbonate films were investigated. The SAXS patterns of both materials exhibit a large number of oscillations in the radial part of the scattering function, indicating excellent pore alignment and a small pore size distribution. Analysis of the SAXS data based on model calculations with cylindrical pores yields information about the pore radii and the radius dispersions as a

function of parameters such as etching time, UV treatment and ion fluence. Comparing the SAXS patterns, the pore quality of LOFO samples is slightly higher than for Makrofol. Moreover, the pore etch rate of LOFO is systematically lower than in Makrofol for the same etching conditions. At present, we cannot assign these differences to a specific material property because of a lack of information from the producer.

We also investigated the effect of UV treatment prior to chemical track etching and could assign the beneficial effect on a reduced size distribution of the etched pores, in particular for short etching times. With increasing pore size and density the quality of the SAXS oscillations decays, indicating interacting pores. This is important information because overlapping channels are known to deteriorate filtration properties.

The authors thank S. Poissonnet and P. Bonnaillie, DMN/SRMP, CEA-Saclay for the high quality electron micrograph in Fig. 1.

### References

- Chtanko, N., Toimil-Molares, M. E., Cornelius, T. W., Dobrev, D. & Neumann, R. (2005). *Nucl. Instrum. Methods B*, **236**, 103–108.
- Cornelius, T. W., Brötz, J., Chtanko, N., Dobrev, D., Mische, G., Neumann, R. & Toimil Molares, M. E. (2005). *Nanotechnology*, **16**, S246–S249.
- Dobrev, D., Baur, D. & Neumann, R. (2005). *Appl. Phys. A Mater. Sci. Process.* **80**, 451–456.
- Ferain, E. & Legras, R. (2003). *Nucl. Instrum. Methods B*, **208**, 115–122.
- Fleischer, R. L., Price, P. B. & Walker, R. M. (1975). *Nuclear Tracks in Solids, Principles and Applications*, ISBN 0-520-04096-1. Berkeley: University of California Press.
- Heins, E. A., Siwy, Z. S., Baker, L. A. & Martin, C. R. (2005). *Nano Lett.* **5**, 1824–1829.
- Mara, A., Siwy, Z., Trautmann, C., Wan, J. & Kamme, F. (2004). *Nano Lett.* **4**, 497–501.
- Metz, S., Trautmann, C., Bertsch, A. & Renaud, P. (2004). *J. Micromech. Microeng.* **14**, 324–331.
- Pépy, G. (2007). *J. Appl. Cryst.* **40**, s433–s438.
- Pépy, G., Balanzat, E., Jean, B., Kuklin, A., Sertova, N. & Toulemonde, M. (2003). *J. Appl. Cryst.* **36**, 649–651.
- Pépy, G. & Kuklin, A. (2001). *Nucl. Instrum. Methods B*, **185**, 198–203.
- Reber, N., Omichi, H., Spohr, R., Wolf, A. & Yoshida, M. (1999). *Nucl. Instrum. Methods B*, **151**, 146–153.
- Riedel, C. & Spohr, R. (1979). *Radiat. Eff.* **42**, 69–75.
- Schiedt, B., Healy, K., Morrison, A. P., Neumann, R. & Siwy, Z. (2005). *Nucl. Instrum. Methods B*, **236**, 109–116.
- Siwy, Z., Apel, P., Dobrev, D., Neumann, R., Spohr, R., Trautmann, C. & Voss, K. (2003). *Nucl. Instrum. Methods B*, **208**, 143–148.
- Siwy, Z., Gu, Y., Spohr, H. A., Baur, D., Wolf-Reber, A., Spohr, R., Apel, P. & Korchev, Y. E. (2002). *Europhys. Lett.* **60**, 349–355.
- Spohr, R. (1980). *Nucl. Instrum. Methods B*, **173**, 229–236.
- Yoshida, M., Nagaoka, N., Asano, M., Omichi, H., Kubota, H., Ogura, K., Vetter, J., Spohr, R. & Katakai, R. (1997). *Nucl. Instrum. Methods B*, **122**, 39–44.